Synthetic Chloride-Selective Carbon Nanotubes Examined by Using Molecular and Stochastic Dynamics

Tamsyn A. Hilder,* Dan Gordon, and Shin-Ho Chung
Research School of Biology, Australian National University, Canberra, Australia

ABSTRACT Synthetic channels, such as nanotubes, offer the possibility of ion-selective nanoscale pores which can broadly mimic the functions of various biological ion channels, and may one day be used as antimicrobial agents, or for treatment of cystic fibrosis. We have designed a carbon nanotube that is selectively permeable to anions. The virtual nanotubes are constructed from a hexagonal array of carbon atoms (graphene) rolled up to form a tubular structure, with an effective radius of 4.53 Å and length of 34 Å. The pore ends are terminated with polar carbonyl groups. The nanotube thus formed is embedded in a lipid bilayer and a reservoir containing ionic solutions is added at each end of the pore. The conductance properties of these synthetic channels are then examined with molecular and stochastic dynamics simulations. Profiles of the potential of mean force at 0 mM reveal that a cation moving across the pore encounters an insurmountable free energy barrier of ~25 kT in height. In contrast, for anions, there are two energy wells of ~12 kT near each end of the tube, separated by a central free energy barrier of 4 kT. The conductance of the pore, with symmetrical 500 mM solutions in the reservoirs, is 72 pS at 100 mV. The current saturates with an increasing ionic concentration, obeying a Michaelis-Menten relationship. The pore is normally occupied by two ions, and the rate-limiting step in conduction is the time taken for the resident ion near the exit gate to move out of the energy well.

INTRODUCTION

One of the potential applications of nanotechnology is to manufacture ion-selective, nanoscale pores that will broadly mimic some of the functions carried out by biological ion channels. Such devices, if successfully engineered, could be used as antimicrobial agents, or could be targeted to specific cell types to modify their functions or render them unviable. Also, engineered nanopores densely embedded in an artificial membrane matrix may serve as ultrasensitive sensors, desalination, or demineralization devices (1,2). Several attempts have been made in the past to design and fabricate nanotubes that can selectively allow water molecules to pass through while rejecting charged particles (3–11). Under the influence of an applied pressure, a narrow nanotube made from a hexagonally packed array of carbon atoms or alternating boron and nitrogen atoms, with a radius ranging from 3.45 to 4.1 Å, is capable of transporting ~6–23 water molecules per ns (5,9,11), the flow rate of which is substantially higher than that of the biological water channel, aquaporin-1 (12). When the radius of the pore is enlarged, the flow rate increases but salt ions also move across the pore, especially at high ionic concentrations (8). The possibility of engineering ion-selective nanotubes has also been explored (13). When a rim of partially charged atoms are placed near the entrance, ions surmount the energy barrier near the open-ended entrance, created by induced surface charges, and move into the interior of a carbon nanotube (14–16). Recently, Hilder et al. (17) showed that boron nitride nanotubes, with radii of 4.83 and 5.52 Å, embedded in a silicon nitride membrane, are selectively permeable to cations and anions, respectively. Won and Aluru (18) show that single-walled boron nitride nanotubes 14 Å in length exhibit ionic selectivity of chloride ions over potassium, whereas the opposite is true for a carbon nanotube of similar diameter and length.

In recent years, the technology of manufacturing nanomaterials has progressed at a rapid rate (19). Because the current techniques used for synthesizing nanotubes do not have total control over diameter and the electronic properties of the nanotubes, postsynthesis separation methods (20,21) are used to select the correct types of nanomaterials for the desired application. Once the desired type of nanotubes is separated, their surface chemistry can be modified at selected sites (22). This process, known as covalent functionalization, increases the utility of the nanotube structure enormously and enhances the molecular selectivity beyond steric sieving effects. By attaching hydrophilic residues on the sidewall, the nanotubes can be rendered soluble (23,24) or they can be made to spontaneously insert into and align across a lipid bilayer (6). Also, a protein can be attached directly on the outer surface of carbon and boron nitride nanotubes (25), and a polymer can be made to wrap around the tube (2,24,26). Given the rapid advances in the methods of fabricating nanomaterials, it may only be a matter of time until practical nanodevices, which are less complex than biological systems but possess the functionality of membrane ion channels, are successfully created and widely utilized. With this potential application in mind, we carry out computational studies, at the proof-of-concept

Submitted March 2, 2010, and accepted for publication June 11, 2010.

*Correspondence: tamsyn.hilder@anu.edu.au

Editor: Gerhard Hummer.

0006-3495/10/09/1734/9 $2.00

doi: 10.1016/j.bpj.2010.06.034

level, on (9, 9) nanotubes of 4.53 Å effective radii constructed from carbon atoms and terminated with carbonyl groups. We demonstrate that it is possible to create practical nanoscale devices which exhibit broadly similar conductance properties as chloride-selective biological membrane ion channels, such as $GABA_A$ receptors (27,28) and ClC-type channels (29,30).

The synthetic nanotubes we describe here present an insurmountable free energy barrier for cations but allow anions to move across under the influence of an applied potential. The energy landscape encountered by an anion is similar to the profile of potential of mean force (PMF) presented to a cation by the gramicidin pore (31–33). At 0 mM ionic concentration, two energy wells of 12 *kT* in depth near the end of the nanotubes are separated by a central energy barrier whose height is ~4 *kT*. Using distributional molecular dynamics (32), we detail the dynamics of ion permeation across the chloride-selective carbon nanotubes and provide their current-voltage-concentration profiles. The current-voltage relationship is nonlinear, the conductance with 500 mM ionic solutions increasing from 72 pS to 96 pS as the applied potential increases from 100 mV to 200 mV, and the pore has a Michaelis-Menten current-concentration relationship. The rate-limiting step in conduction is the time taken for the resident ion in the energy well near the exit gate to move out of the energy well. In addition, we illustrate that these carbonyl-terminated carbon nanotubes are stable in a lipid bilayer.

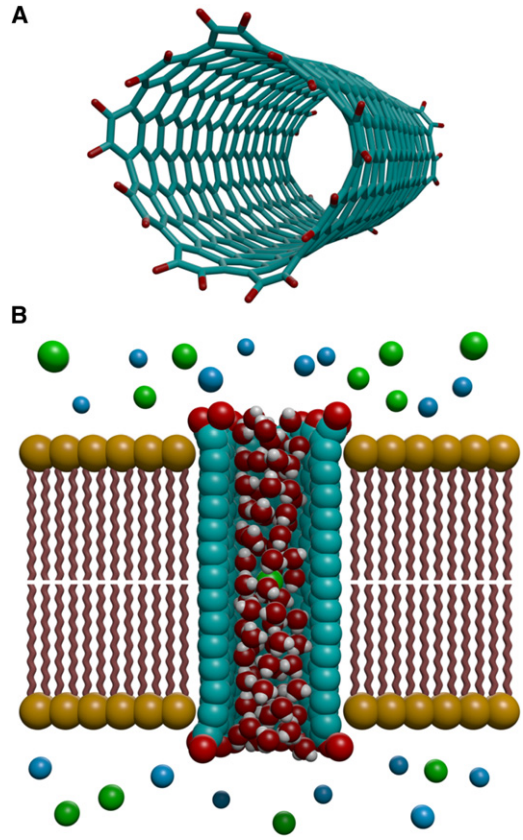

FIGURE 1 Schematic of the (9, 9) carbon nanotube with (*A*) oxygen-terminated ends (shown in *red*) and (*B*) embedded in a lipid bilayer. Note that for clarity, water in the reservoirs is not shown.

METHODS

Two main computational tools we use for this study are molecular dynamics (MD) and distributional molecular dynamics (DMD) (32,34). Distributional molecular dynamics (32), so named because its main aim is to reproduce the distribution of ion trajectories implicit in MD as closely as possible, combines molecular and stochastic dynamics and enables the permeation of ions across these artificial channels to be determined at much longer timescales than would be possible by using MD simulations (on the order of several nanoseconds to microseconds). Briefly, the free energy profile (or PMF) determined from MD simulations and the distribution of frictional and random forces that are measured over discrete segments of the channel are incorporated into stochastic simulations based on the nonlinear generalized Langevin equation. By using this method, we are able to generate current-voltage-concentration curves and determine ion binding sites within the nanotube.

Construction of nanotubes

Single-walled carbon nanotubes were constructed from a hexagonal array of carbon atoms rolled up to form a tubular structure with physical properties given by Dresselhaus et al. (35). The etching process involved in fabricating open-ended nanotubes introduces either hydroxyl (OH), carbonyl (C=O), or carboxylic (COOH) functional groups to the nanotube ends (8,36). As such, the nanotube ends were terminated with double-bonded oxygen atoms using a O=C bond length (37) of 1.24 Å.

As a first approximation, a partial charge of −0.51 e was applied to each oxygen atom, and 0.51 e to each carbon atom directly bonded to the oxygens using the double-bonded oxygen-carbon group given in the CHARMM27 force field (38,39). The charge assigned to the carbon and oxygen atoms of the carbonyl group in the GROMOS force field are, respectively, 0.38 e and −0.38 e (40), considerably smaller than those used in the CHARMM27 force field. In addition, Hou et al. (41) determine a partial charge of −0.3 *e* on the oxygen atoms from quantum chemistry calculations. Thus, the partial charges used in this model represent an approximation. To examine the effect of partial charge we run simulations using charges from both the GROMOS force field (±0.38 e) and the CHARMM27 force field (±0.51 e). Additional ab initio studies are required to determine exact charges on the carbon and oxygen atoms, using the procedures detailed in a previous study on boron nitride nanotubes (42).

Carbon nanotubes are defined by their chiral vector, $\mathbf{C} = n\mathbf{a_1} + m\mathbf{a_2} = (n, m)$, where $\mathbf{a_1}$ and $\mathbf{a_2}$ represent the unit vectors of the hexagonal lattice and *n* and *m* are integers. We consider only armchair type nanotubes, which are defined as (*n*, *n*). Specifically, we investigated (9, 9) carbon nanotubes with a total length of 34 Å, and an effective radius of 4.53 Å as illustrated in Fig. 1 *A*. This length was chosen to investigate the effect in eukaryotic membranes. It is now technically feasible to synthesize carbon nanotubes with pore diameters as small as, or smaller than, the one we consider in this study (19). In our study, the carbon/carbon pore diameter is ~12 Å. Single-walled carbon nanotubes with diameters ranging from 11 to 15 Å have been successfully fabricated using electric-arc-discharge (43). Nikolaev et al. (44) were able to produce single-wall carbon nanotubes with diameters as small as 7 Å using gas-phase catalytic growth. More recently, Li et al. (45) synthesized 4 Å diameter single-walled carbon nanotubes using a molecular sieve as a template. The carbon nanotube was modeled using a carbon-carbon bond distance of 1.42 Å (35), and the parameters for an aromatic ring from the CHARMM27 force field (38,39).

Molecular dynamics simulation

Molecular dynamics (MD) simulations were performed using NAMD (34) and visualized using VMD (46). We conducted MD simulations to

1. Determine the free energy profile and distribution of frictional and random forces.
2. To investigate the stability of the carbon nanotube in the lipid bilayer using steered molecular dynamics.

Free energy

The MD domain consisted of a carbon nanotube embedded in a palmitoyl-oleoyl-phosphatidylethanolamine (POPE) lipid bilayer between two reservoirs containing water and ions (sodium and chloride), as illustrated in Fig. 1 *B*. The carbon atoms of the nanotube were constrained using a fairly rigid harmonic constraint of 0.25 kcal mol^{-1} Å^{-2}. A constraint of similar magnitude is applied in previous work on carbon nanotubes (9,10). Furthermore, it is reasonable to constrain the tilting motion of the nanotube in the bilayer because previous studies (6,47) have shown that hydrophilic functional end groups, such as those proposed in this article, help to stabilize the nanotube in the bilayer. No constraints were applied to the lipid bilayer. Molecular dynamics simulations were conducted at an NaCl ionic concentration of 0 mM. In other words, only the ion of interest was present in the simulation. This enabled the three-dimensional PMF to be used directly in subsequent DMD simulations while avoiding double-counting the effects of background ions. As a result of including the ion of interest only, the system will have a nonneutral charge. With particle-mesh Ewald electrostatics, this will have the effect of a homogeneous neutralizing background charge filling the entire simulation space (48). Although this will affect the free energy, its effect is negligible for a nonneutral charge of 1 *e*. From Kastenholz and Hünenberger (48), the offset of the electrostatic free energy for our model is estimated as $-0.16\,kT$. This offset is only present when there is a nonneutral unit cell, and is essentially a result of the interaction of the solute charges with their own periodic copies and the neutralizing background charge.

The CHARMM27 (38,39) force field, and the TIP3P water model were used in all simulations. The system was replicated periodically in all three dimensions and particle-mesh Ewald electrostatics was used. The simulation box was ~58 × 58 × 76 Å^3 and contained 4598 water molecules, and either one sodium or one chloride ion. Each system was equilibrated for 1 ns at a constant temperature of 310 K and a constant pressure of 1 bar. The three-dimensional potential of mean force (PMF) of the specific ion moving through the nanotube was determined using umbrella sampling. Given that the nanotube is symmetric, the ion positions were sampled only in the positive z domain, and reflected to obtain the negative z PMF. The ion was moved through positions from 0 to 30 Å in 0.5 Å increments and the z component held using a harmonic constraint of 12.5 kcal mol^{-1} Å^{-2} whereas the ion was free to move radially. This harmonic constraint was chosen to give sufficient overlap between each window and its neighbors while constraining the ions enough to ensure adequate sampling of the entire reaction coordinate. The ion's z and radial coordinates were obtained during each umbrella sampling run of 1 ns, and the data were analyzed using the weighted histogram analysis method (WHAM) (49,50), to obtain a two-dimensional PMF with reaction coordinates (z, r). Finally, this two-dimensional PMF was converted thermodynamically into a three-dimensional, radially symmetric PMF.

Steered molecular dynamics

To determine whether the carbon nanotube with its ends terminated with polar carbonyl groups can be embedded across and remain stable in the lipid bilayer, we perform steered molecular dynamics (SMD) simulations and calculate the changes in the free energy as the tube is slowly pulled away from the membrane. If the tube experiences a negative free energy shift as it is inserted into the bilayer, then the tube will be stable inside the bilayer. We begin with an equilibrated system containing the oxygen-terminated nanotube with a nominal length of 34 Å embedded in a POPE lipid bilayer consisting of 55 lipid chains. The system is hydrated by a 250 mM NaCl solution containing 6655 water molecules and 31 NaCl pairs. Constant pressure dynamics are used to maintain the pressure at 1 bar, which results in a periodic cell size of ~49 × 49 × 111 Å^3. Various restraints are applied to the nanotube and bilayer to control the progress of the steered molecular dynamics simulation. The center-of-mass of the nanotube is harmonically constrained to the origin in the x-y plane with a spring constant of 250 kcal mol^{-1} Å^{-2}, and the z component of the bilayer center-of-mass is likewise constrained to $z = 0$ with a spring constant of 250 kcal mol^{-1} Å^{-2}. These constraints should not affect the energy calculation, due to the symmetry and periodicity of the system. As a first approximation, the tilt angle of the tube is furthermore strongly constrained to lie parallel to the z axis and perpendicular to the lipid membrane.

The SMD simulation itself is controlled by defining a reaction coordinate as being the projection onto the z axis of the vector joining the lipid and nanotube centers-of-mass. This reaction coordinate is then constrained to a moving point that is initially at the origin and moves in the positive z direction with a velocity $v_z = 10$ Å/ns. The spring constant for this SMD pulling constraint is 5000 kcal mol^{-1} Å^{-2}, which is large enough to ensure that the reaction coordinate closely follows the moving target. As the simulation progresses, the projected system forces on the reaction coordinate are collected. For each simulation, the total work in moving from $z = 0$ to $z = z_f$ is then found to be

$$W(z_f) = \int_{z=0}^{z_f} f(z)dz, \tag{1}$$

where $f(z)$ is the force on the reaction coordinate at z. If the tube is pulled out of the lipid slowly enough that the process is quasistatic, then this work will be equal to the PMF. In reality, there will be some unknown dissipative component to the work. This can be partially corrected for by employing more than one simulation and using Jarzynski's equality (51), which derives the free energy from an ensemble of nonequilibrium trajectories. The simulations were run with a 2-fs timestep.

Distributional molecular dynamics

In a narrow conduit formed by carbon atoms, water molecules are ordered and not free to align with the external field. In such a mesoscopic system, the solution of Poisson's equation with any assumed pore dielectric constant will not accurately provide the magnitude of the force impinging on a permeant ion. Also, the mobility of the ion (as well as the stochastic force impinging on it) in different segments of the tube is likely to vary along the conduction pathway. The conductance of the nanotube should ideally be determined by using molecular dynamics which uses explicit solvent, but it is computationally intractable to construct the current-voltage-concentration profiles with this method. To overcome these difficulties for modeling the permeation of ions across a nanotube, we have devised a new methodology called distributional molecular dynamics (DMD) that combines molecular dynamics and stochastic dynamics (32), and uses implicit solvent. The theoretical basis for this procedure and a detailed test using gramicidin-A are given by Gordon et al. (32).

Initially, molecular dynamics is used to determine a free energy profile for the ion in the nanotube, and the distribution of random and frictional forces is measured over discrete segments of the tube. In doing this, we are able to match the distribution of ion trajectories in DMD as closely as possible to MD. The parameters thus determined are used in stochastic dynamic simulations based on the nonlinear generalized Langevin equation, given by

$$\begin{aligned}\partial_t \mathbf{q}(t) &= m^{-1}\mathbf{p}(t),\\ \partial_t \mathbf{p}(t) &= \mathbf{F}_{\mathrm{D}}(\mathbf{q}(t)) - \int_0^t dt' K(t')\mathbf{p}(t-t') + \mathbf{F}_{\mathrm{R}}(t),\end{aligned} \tag{2}$$

where $\mathbf{q}(t)$ and $\mathbf{p}(t)$ are the coordinate and momentum at time t, respectively; m is the mass; $\mathbf{F_D}$ represents the deterministic force or, in this case, the three-dimensional PMF; and the second term represents the frictional force in which $K(t')$ is the friction kernel. The last term $\mathbf{F_R}$ is the random force which is assumed to be a Gaussian random force related to the friction kernel through the fluctuation-dissipation theorem, which is given by

$$\left\langle F_R(0)F_R^T(t)\right\rangle = kTK(t)m, \tag{3}$$

where k and T assume the usual significance.

To prevent double-counting of the interaction between any given ion and the net effect of all the other ions, we perform our MD simulation at 0 mM to generate the PMF, or deterministic force used in DMD. In future work we hope to compare the PMF obtained from DMD at finite ion concentrations with that obtained from MD. Preliminary work suggests that the two compare well. All ion-ion related effects are a result of the macroscopic electrostatics that are built into the stochastic simulation.

The simulation space is divided into two regions, namely a channel region and a bulk region. In the channel region, the nonlinear generalized Langevin equation (Eq. 2) is solved with a 1-fs timestep, using the friction kernel determined from MD. In the bulk region, normal Brownian dynamics is used with a 100-fs timestep. All single-ion deterministic forces are derived from the PMF taken from MD; these represent the interactions between a single ion and the nanotube/membrane system. In contrast, ion-ion interactions are calculated using macroscopic electrostatics (Poisson's equation with a dielectric barrier defined by the nanotube/membrane system) plus other fitted short-range, ion-ion forces.

As mentioned, the PMF is determined using WHAM (49,50). The data gathered for the WHAM is also used to determine the friction kernel, $K(t)$. For each ion trajectory we determine the momentum autocorrelation function $C(t)$ and derive $K(t)$ using

$$\partial_t C = -\int_0^t K'(t-t')C(t')dt'. \tag{4}$$

The inverse velocity decay time due to friction, γ, is then determined as the time integral of $K(t)$ from $t = 0$ to $t = \infty$. Note that the diffusion coefficient can be determined using γ and the Einstein relation $D = kT/(m\gamma)$, where D is the diffusion coefficient and m is the mass. Thus, using this relation we can represent the diffusion coefficient within the tube, as illustrated in Fig. 2 *A*. As can be seen from Fig. 2 *A* the diffusion coefficient of chloride increases inside the nanotube and once outside the nanotube reduces back to approximately that of bulk (2.03×10^{-9} m^2/s) (52). We then assume the friction kernel can be approximated by an exponential function, thus

$$K(t) = \gamma\kappa\exp(-\kappa t), \tag{5}$$

so as to determine the inverse decay time of the friction memory kernel, κ. Fig. 2 *B* illustrate how κ varies along the length of the nanotube.

In summary, three parameters that feature in the generalized Langevin equation are the deterministic force, $\mathbf{F_D}$; random force, $\mathbf{F_R}$; and frictional force, $\mathbf{F_F}$. The latter two forces represent the stochastic force arising from random collisions of an ion with its surrounding molecules. In Brownian dynamics, these parameters are estimated by solving Poisson's equation and by using the fluctuation-dissipation theorem (53). In DMD, the pore is divided into thin slices, and the forces acting on an ion and the diffusion coefficient in each section are obtained from a three-dimensional PMF and friction kernel taken from MD. This ensures that for a single ion certain properties of the trajectory in MD, such as the probability of finding the ion at a given position, will be reproduced in DMD. When there are two ions in the pore, the interactions between them are treated by using macroscopic electrostatics. Poisson's equation is solved to determine the ion-ion interaction with the results for all possible configurations of two ions being stored in a lookup table which is consulted during the simulation (53).

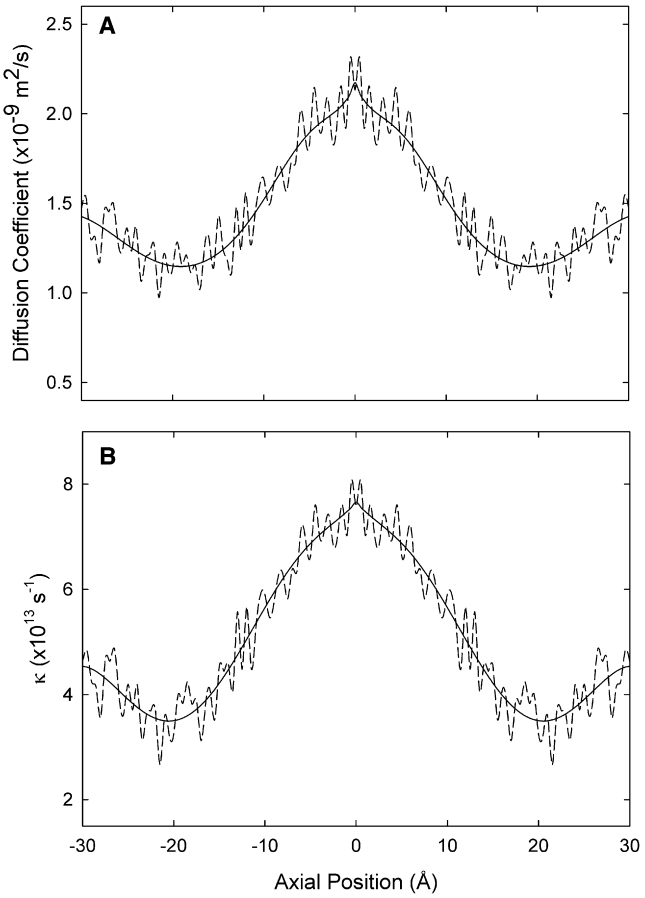

FIGURE 2 Distributional molecular dynamics parameters for chloride in the (9, 9) carbon nanotube. (*A*) Variation in the diffusion coefficient. (*B*) Inverse decay time of the friction memory kernel, κ. (*Solid line*) Average value.

All current-voltage curves were generated at an ionic concentration of 500 mM. Current was calculated using the relationship $I = qn/\Delta t$, where n is the average number of ions that cross the membrane, q is the charge of the ion, and Δt is the simulation time of one run. Current-concentration curves were generated at a voltage of 200 mV.

RESULTS AND DISCUSSION

Channel topology and membrane entry

We investigate (9, 9) single-wall carbon nanotubes with a total length of 34 Å embedded in a lipid bilayer separating two reservoirs (Fig. 1 *B*). This length corresponds to that of eukaryotic cell membranes. As part of the fabrication of open-ended nanotubes, carbonyl (C=O) functional groups are introduced to the nanotube ends (8) (Fig. 1 *A*). As a result of the uncertainty as to the exact partial charges to be placed on the carbonyl group, we have examined the effect of

partial charge variation by running two sets of simulations with the charge on the carbonyl groups set to 1), ±0.38 e and 2), ±0.51 e, which are the charges determined by the GROMOS (40) and CHARMM27 force fields (38,39), respectively. As such, each end of the carbon nanotube is functionalized with 36 oxygen atoms each carrying a charge of either −0.38 e or −0.51 e, which are double-bonded to the last ring of carbon atoms each carrying a charge of either 0.38 e or 0.51 e. The nanotube can be considered a perfectly cylindrical nonpolar channel with an approximate effective radius of 4.53 Å with polar-terminated ends. These polar ends assist in chloride conduction and maintain stability of the nanotube in the lipid bilayer (6,47).

The channel is composed of three regions:

1. The nonpolar center of the nanotube.
2. The carbon atoms at the nanotube end which are positively charged.
3. The oxygen-terminated ends.

The average radius within these three regions varies. Inside the nanotube in region 1, the average effective radius of carbon atoms is 4.53 Å. The carbon atoms at the nanotube ends in region 2 get shifted outwards as a result of the end functionalization and their average effective radius is 4.78 Å. Finally, the oxygen-terminated ends point outwards from the end and have an average effective radius of 5.09 Å. In other words, the positively charged carbon atoms at the nanotube mouth are exposed to ions approaching the channel. It is expected that as the ionic concentration increases there may be some screening of these polar-terminated ends.

Coarse-grained molecular dynamics studies show that carbon nanotubes with hydrophilic residues attached to their ends spontaneously insert into and align across a lipid bilayer (6,54). These hydrophilic functional groups, such as the double-bonded oxygen functional groups, are shown to stabilize the nanotube in the bilayer (6,47) and it is essential that they be closely matched with the hydrophilic groups of the lipid bilayer for the transport of ions to occur without pore occlusion (6). The transport of the hydrophilic nanotube ends through the hydrophobic membrane inner core is facilitated by lipids which act to chaperone the nanotube ends through the membrane (6,55).

We investigated the membrane entry of our carbonyl-terminated carbon nanotubes using an alternate approach, namely steered molecular dynamics. By pulling the nanotube through the bilayer, we were able to generate a free energy profile, as illustrated in Fig. 3. There is a large energy well of between 250 and 300 kcal mol^{-1} confining the nanotube to the center of the lipid membrane. Therefore, we conclude that the nanotube is likely to be stable in the lipid membrane. The agreement between the curve calculated using a pulling speed of 2.5 Å/ns and the curve calculated using a pulling speed of 5 Å/ns suggests that the pulling speed is low enough to ensure that the energy calculation has converged. Having not calculated the effect of rotating the nanotube, we cannot preclude the possibility that there is some even more stable configuration (for example with the tube lying parallel to the lipid membrane). However, the work of Lopez et al. (6), which uses coarse-grained molecular dynamics to examine the insertion dynamics of a generic carbon nanotube with hydrophilic ends, provides evidence against this possibility.

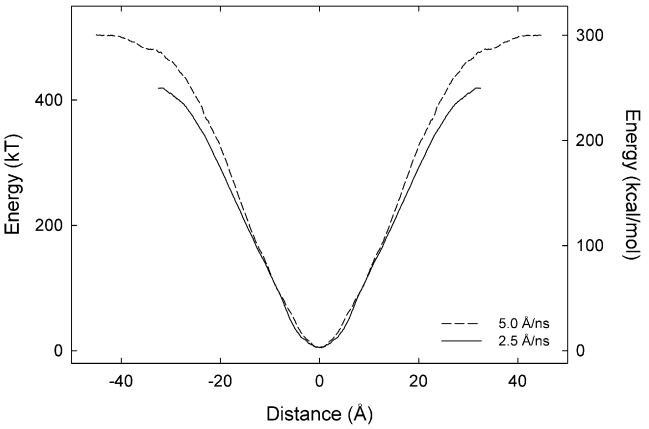

FIGURE 3 Free energy profile as a function of the z distance between the nanotube and lipid bilayer centers-of-mass. Note that the pulling speed of 2.5 and 5 Å/ns is shown.

Energy profiles

Fig. 4, *A* and *B*, illustrates the free energy profiles at 0 mM ionic concentration of sodium and chloride ions, respectively, for the (9, 9) carbon nanotube with a carbonyl group charge of ±0.38 e and ±0.51 e. Note that the free energy profile shown here is derived from the three-dimensional PMF and is therefore the free energy of the ion as it moves along the nanotube axis. For a carbonyl group charge of ±0.51 e, an insurmountable free energy barrier of ~25 kT exists for sodium ions: thus, sodium ions are not expected to traverse through the nanotube. This barrier arises primarily from the functional end group of the nanotube which act as a barrier to cations. On the other hand, the energy profile for chloride ions consists of two energy wells of ~12 kT at either end of the nanotube separated by a central energy barrier of ~4 kT. The two wells are situated at approximately the location of the first row of carbon atoms, which are positively charged due to the oxygen-terminated ends. Using Poisson's equation, it is possible to construct a simple energy profile which describes the interaction between an ion with the partial charges on the nanotube. In the absence of a membrane potential, this calculation demonstrates qualitative agreement with the energy profiles presented in this article.

As shown in Fig. 4, *A* and *B*, the magnitude of the free energy barriers and wells are reduced when the carbonyl group charge is changed from ±0.51 e to ±0.38 e. When

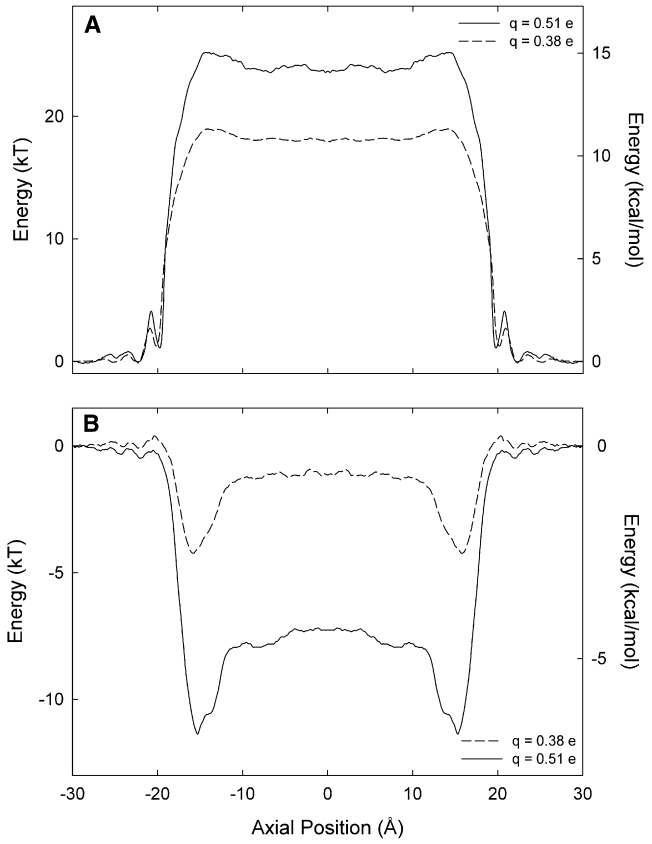

FIGURE 4 Free energy profile of (*A*) sodium (Na^+) and (*B*) chloride (Cl^-) ions for the (9, 9) carbon nanotube with a length of 34 Å at 0 mM ionic concentration and using the carbonyl charge from the CHARMM27 force field (±0.51 e) and GROMOS force field (±0.38 e).

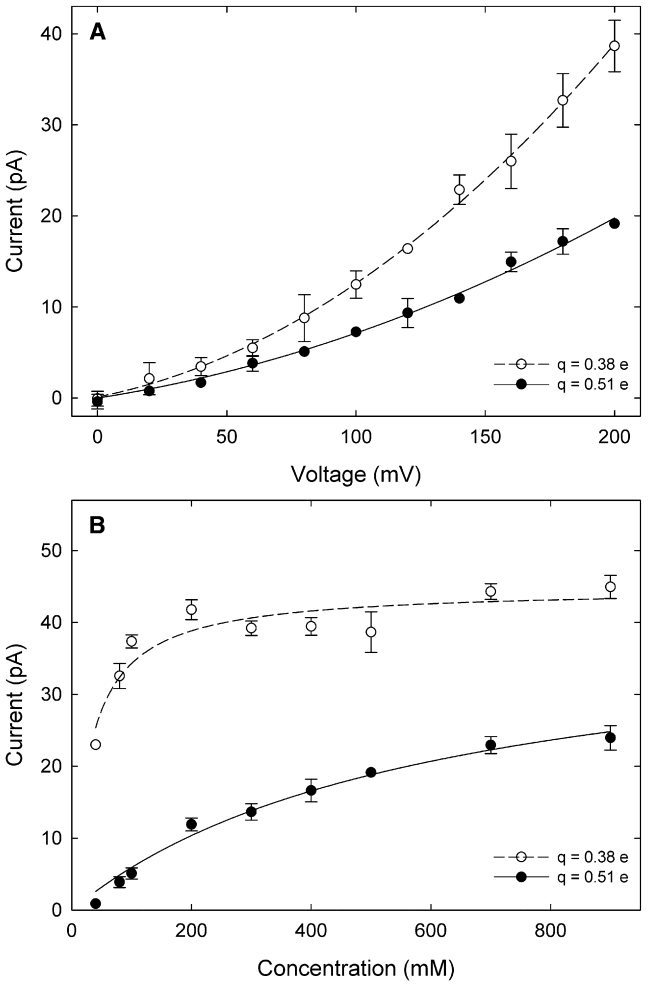

FIGURE 5 Current-voltage-concentration profiles for (9, 9) carbon nanotube 34 Å in length. (*A*) Current-voltage profile generated at an ionic concentration of 500 mM, and (*B*) current-concentration profile generated at a voltage of 200 mV of chloride ions. Each data point represents the average of five sets of simulations, each simulation lasting 8×10^6 time-steps (0.8 μs). Error bars represent two standard errors of the mean and error bars smaller than the data points are not shown.

the charge is reduced, the free energy barrier for sodium ions (Fig. 4 *A*) reduces from 25 *kT* to ~18 *kT*. Similarly, in the free energy profile for chloride ions (Fig. 4 *B*), the reduced charge results in the two energy wells at either end of the nanotube decreasing from 12 *kT* to ~4 *kT* separated by a central energy barrier of ~3 *kT*. The central energy barrier is similar in both cases.

In this study, we place the carbon nanotube in the lipid bilayer, which has a low dielectric constant. Although we have not investigated the conductance properties of the nanotube placed in a different matrix, we expect to obtain similar results when the nanotube is embedded in any similar low dielectric medium. This assertion is based on the fact that the current-voltage relationships obtained from the KcsA and MthK potassium channels are shown to be relatively insensitive to the assumed dielectric constant of the protein (56,57).

Current-voltage-concentration profile

The current-voltage profile for the (9, 9) nanotube of 34 Å length with a carbonyl group charge of ±0.38 e and ±0.51 e is shown in Fig. 5 *A*. Unlike the chloride-selective ion channels (27,29) and the gramicidin pore (31), the current-voltage relationship is slightly nonlinear for both investigated carbonyl charges. For example, with a carbonyl group charge of ±0.51 e, at 100 mV the chloride conductance is 72 pS, and as the voltage is increased to 200 mV the conductance increases to 96 pS. Similarly, with a carbonyl group charge of ±0.38 e the chloride conductance increases from 125 pS at 100 mV to 193 pS at 200 mV. This deviation of the current-voltage relationship from Ohm's law results from the presence of a central barrier. An energy barrier an ion needs to surmount becomes less of an impediment when the driving force becomes larger. The current across the engineered pore (±0.51 e carbonyl groups) at an applied potential of 100 mV is 7.2 pA, which is larger than the measured currents at the same applied potential

from ClC-1 (29), gramicidin channels (31,58), and $GABA_A$ receptor (28). The currents across these three biological ion channels are, respectively, 1.8, 2.3, and 4.6 pA at 100 mV and 500 mM. In addition, the current across the engineered pore at an applied potential of 100 mV increases from 7.2 to 12.5 pA as the carbonyl group charge is reduced from ± 0.51 to ± 0.38 e. We note that even at the highest voltage of 200 mV no sodium conduction was observed for both investigated carbonyl charges.

Fig. 5 *B* illustrates the current-concentration profile. For a carbonyl charge of ± 0.51 e, the current gradually saturates with an increasing ionic concentration by following a Michaelis-Menten form,

$$I = I_{max}/(1 + [Cl_s]/[Cl]),$$

where the current I approaches the saturation current I_{max} when the concentration [Cl] is much larger than the half-saturation concentration $[Cl_s]$. Specifically, the current approaches the saturation current, I_{max} at 41 pA, and the half-saturation point occurs at a concentration of 600 mM. This kind of relationship occurs when there are concentration-dependent and concentration-independent steps involved in the ion conduction mechanism (28). It is expected that the time spent waiting for an ion to enter the channel will decrease as the concentration increases, but the time it takes for an ion to overcome the barrier to exit will remain unchanged. For a carbonyl charge of ± 0.38 e the current very quickly saturates with an increasing ionic concentration, again following a Michaelis-Menten form. Now the current approaches the saturation current I_{max} at 45 pA, and the half-saturation point occurs at a concentration of 31 mM. The nanotube pore saturates more quickly with increasing concentration with a charge of ± 0.38 e on the carbonyl group because the chloride ions are no longer restricted by a large energy barrier to exit the pore. Similar to the current-voltage curve, no sodium conduction was observed for all concentrations and carbonyl group charges investigated.

Ions in the channel and the conduction mechanism

To elucidate the detailed processes by which a conduction event takes place, we examine the locations of binding sites in the pore and how a resident ion transits from one binding site to another for the case where a partial charge of ± 0.51 e is applied to the carbonyl groups. We divide the (9, 9) nanotube 34 Å in length into 50 thin sections and compute the time averages of chloride ions in each section during the simulation period of 4 μs. In the absence of an applied potential, resident ions tend to dwell preferentially near the pore entrances, at the location of two energy wells (Fig. 4 *B*), as shown in Fig. 6. On average, 1.3 chloride ions occupy each well. Thus, there are two resident ions

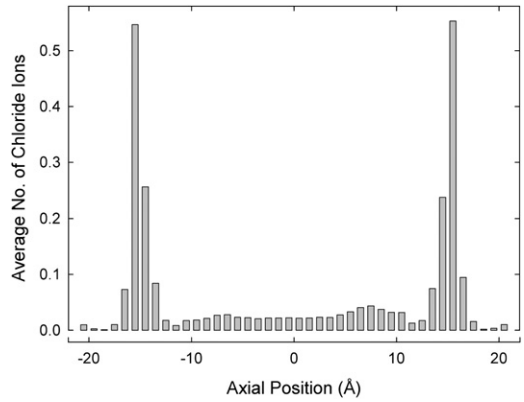

FIGURE 6 Binding sites of chloride ions for the (9, 9) carbon nanotube in the absence of an applied potential and using the carbonyl charge from the CHARMM27 force field (± 0.51 e).

in the pore, which, with the aid of the repulsive force exerted by a third ion and an applied potential, are ready to move into the reservoir. In contrast, no sodium ions occupy the nanotube interior for the entire simulation.

Translocation of an ion across the pore is achieved, not by a slow and gradual diffusive motion, but by an ion jumping from one binding site to another, the probability of a hop being determined by the energy difference between the sites and the available thermal energy. To detail this process, the axial position of every ion in the pore is recorded at each timestep during each DMD simulation. These positions are then used to determine the ion configuration in the tube, where each binding site is either filled [1] or empty [0], and the ion moves from positive to negative z. Initially, an ion in the reservoir under the influence of an applied potential of 100 mV enters the first binding site. A second ion approaching the binding site causes the first ion to jump to the second binding site, and the two resident ions in the binding sites establish a stable equilibrium. The pore is in this configuration almost all of the time. A conduction event occurs when a third ion enters the first energy well. The outermost ion is expelled from the pore through a knock-on effect or Coulomb repulsion. Once again, the rate-limiting step in conduction in this engineered pore is the barrier presented to the resident ion in the energy well near the exit gate to climb out of the well. This confirms the same conduction mechanism as the current-voltage-concentration profiles.

We also examined the conduction mechanism at the reduced charge (± 0.38 e). As expected, due to the reduced energy wells present for the charge of ± 0.38 e, there are now, on average, only 0.93 chloride ions occupying each well so that there are almost two resident ions in the pore. Similar to the carbonyl charge of ± 0.51 e, no sodium ions occupy the nanotube interior for the entire simulation. In addition to the slight decrease in the number of ions present in nanotube pore, reducing the charge from 0.51 to 0.38 also decreases the time the pore has two resident

ions from almost all of the time, to 85%. Despite these small differences, the conduction mechanism is identical for both carbonyl charges considered in this article.

CONCLUSIONS

We show that a (9, 9) carbon nanotube with an effective radius of 4.53 Å and length of 34 Å terminated with polar carbonyl groups is stable in a lipid bilayer and is selective to chloride ions. Confirming the results of previous work (6,47), by using SMD we demonstrate that the nanotube is stable in the lipid bilayer. However, our result is limited in that we do not include the effect of nanotube tilting. The chloride selectivity is dependent on the oxygen-terminated ends which, with a partial charge of ± 0.51 e applied to the carbonyl groups, generate an energy well of 12 kT for chloride ions at the entrance and exit of the tube and a large energy barrier of 25 kT for sodium ions. This nanotube has a current of 7.2 pA at 100 mV which is four times larger than the conductance through the ClC-1 channel and almost twice that of $GABA_A$. In addition, the current across the engineered pore at an applied potential of 100 mV increases from 7.2 to 12.5 pA as the carbonyl group charge is reduced from ± 0.51 to ± 0.38 e. The current-concentration profile is found to obey a Michaelis-Menten relationship. The rate-limiting step in conduction is the time taken for the resident ion near the exit gate to move out of the energy well. This artificial channel shows a striking resemblance to a biological ion channel and has the potential to lead to numerous drugs designed to target ion channels, for example for treatments such as antibacterial, and cystic fibrosis.

We gratefully acknowledge the support from the National Health and Medical Research Council and the MAWA Trust. Rhys Hawkins from the Visualization Laboratory at the Australian National University and Silvie Ngo provided excellent technical assistance, for which we are grateful. The calculations upon which this work is based were carried out using the Sun X6275 blades and SGIAltix clusters of the Australian National University Supercomputer Facility.

REFERENCES

1. Rasaiah, J. C., S. Garde, and G. Hummer. 2008. Water in nonpolar confinement: from nanotubes to proteins and beyond. *Annu. Rev. Phys. Chem.* 59:713–740.
2. Qu, L., K. M. Lee, and L. Dai. 2006. Functionalization and applications of carbon nanotubes. *In* Carbon Nanotechnology. Elsevier, Amsterdam, The Netherlands.
3. Hummer, G., J. C. Rasaiah, and J. P. Noworyta. 2001. Water conduction through the hydrophobic channel of a carbon nanotube. *Nature.* 414:188–190.
4. Waghe, A., J. C. Rasaiah, and G. Hummer. 2002. Filling and emptying kinetics of carbon nanotubes in water. *J. Chem. Phys.* 117:10789–10795.
5. Kalra, A., S. Garde, and G. Hummer. 2003. Osmotic water transport through carbon nanotube membranes. *Proc. Natl. Acad. Sci. USA.* 100:10175–10180.
6. Lopez, C. F., S. O. Nielsen, …, M. L. Klein. 2004. Understanding nature's design for a nanosyringe. *Proc. Natl. Acad. Sci. USA.* 101:4431–4434.
7. Majumder, M., N. Chopra, …, B. J. Hinds. 2005. Nanoscale hydrodynamics: enhanced flow in carbon nanotubes. *Nature.* 438:44.
8. Fornasiero, F., H. G. Park, …, O. Bakajin. 2008. Ion exclusion by sub-2-nm carbon nanotube pores. *Proc. Natl. Acad. Sci. USA.* 105:17250–17255.
9. Corry, B. 2008. Designing carbon nanotube membranes for efficient water desalination. *J. Phys. Chem. B.* 112:1427–1434.
10. Garate, J. A., N. J. English, and J. M. D. MacElroy. 2009. Carbon nanotube assisted water self-diffusion across lipid membranes in the absence and presence of electric fields. *Mol. Simul.* 35:2–12.
11. Hilder, T. A., D. Gordon, and S. H. Chung. 2009. Salt rejection and water transport through boron nitride nanotubes. *Small.* 5:2183–2190.
12. Agre, P. 2004. Aquaporin water channels (Nobel Lecture). *Angew. Chem. Int. Ed. Engl.* 43:4278–4290.
13. Peter, C., and G. Hummer. 2005. Ion transport through membrane-spanning nanopores studied by molecular dynamics simulations and continuum electrostatics calculations. *Biophys. J.* 89:2222–2234.
14. Joseph, S., R. J. Mashl, …, N. R. Aluru. 2003. Electrolytic transport in modified carbon nanotubes. *Nano Lett.* 3:1399–1403.
15. Majumder, M., N. Chopra, and B. J. Hinds. 2005. Effect of tip functionalization on transport through vertically oriented carbon nanotube membranes. *J. Am. Chem. Soc.* 127:9062–9070.
16. Park, J. H., S. B. Sinnott, and N. R. Aluru. 2006. Ion separation using a Y-junction carbon nanotube. *Nanotechnology.* 17:895–900.
17. Hilder, T. A., D. Gordon, and S. H. Chung. 2009. Boron nitride nanotubes selectively permeable to cations or anions. *Small.* 5:2870–2875.
18. Won, C. Y., and N. R. Aluru. 2009. A chloride ion-selective boron nitride nanotube. *Chem. Phys. Lett.* 478:185–190.
19. O'Connell, M. J., editor. 2006. Carbon Nanotubes: Properties and Applications. Taylor & Francis, New York.
20. Krupke, R., and F. Hennrich. 2005. Separation techniques for carbon nanotubes. *Adv. Eng. Mater.* 7:111–116.
21. Tromp, R. M., A. Afzali, …, Z. Chen. 2008. Novel strategy for diameter-selective separation and functionalization of single-wall carbon nanotubes. *Nano Lett.* 8:469–472.
22. Wong, S. S., E. Joselevich, …, C. M. Lieber. 1998. Covalently functionalized nanotubes as nanometer-sized probes in chemistry and biology. *Nature.* 394:52–55.
23. Bahr, J. L., and J. M. Tour. 2002. Covalent chemistry of single-walled carbon nanotubes: a review. *J. Mater. Chem.* 12:1952–1958.
24. Tasis, D., N. Tagmatarchis, …, M. Prato. 2003. Soluble carbon nanotubes. *Chemistry.* 9:4000–4008.
25. Zhi, C., Y. Bando, …, D. Golberg. 2005. Immobilization of proteins on boron nitride nanotubes. *J. Am. Chem. Soc.* 127:17144–17145.
26. Zhi, C., Y. Bando, …, D. Golberg. 2005. Perfectly dissolved boron nitride nanotubes due to polymer wrapping. *J. Am. Chem. Soc.* 127:15996–15997.
27. Bormann, J., O. P. Hamill, and B. Sakmann. 1987. Mechanism of anion permeation through channels gated by glycine and γ-aminobutyric acid in mouse cultured spinal neurones. *J. Physiol.* 385:243–286.
28. O'Mara, M. L., B. Cromer, …, S. H. Chung. 2005. Homology model of the $GABA_A$ receptor examined using Brownian dynamics. *Biophys. J.* 88:3286–3299.
29. Miller, C. 1982. Open-state substructure of single chloride channels from *Torpedo electroplax*. *Philos. Trans. R. Soc. Lond. B Biol. Sci.* 299:401–411.
30. Corry, B., M. O'Mara, and S. H. Chung. 2004. Conduction mechanisms of chloride ions in ClC-type channels. *Biophys. J.* 86:846–860.
31. Edwards, S., B. Corry, …, S. H. Chung. 2002. Continuum electrostatics fails to describe ion permeation in the gramicidin channel. *Biophys. J.* 83:1348–1360.

32. Gordon, D., V. Krishnamurthy, and S. H. Chung. 2009. Generalized Langevin models of molecular dynamics simulations with applications to ion channels. *J. Chem. Phys.* 131:134102.
33. Krishnamurthy, V., M. Hoyles, …, S. H. Chung. 2006. Permeation in gramicidin ion channels by directly estimating the potential of mean force using Brownian dynamics simulations. *J. Comput. Theoret. Nanosci.* 3:702–711.
34. Kalé, L., R. Skeel, …, K. Schulten. 1999. NAMD2: greater scalability for parallel molecular dynamics. *J. Comput. Phys.* 151:283–312.
35. Dresselhaus, M. S., G. Dresselhaus, and R. Saito. 1995. Physics of carbon nanotubes. *Carbon.* 33:883–891.
36. Lin, T., V. Bajpai, …, L. Dai. 2003. Chemistry of carbon nanotubes. *Aust. J. Chem.* 56:635–651.
37. Kim, C., K. Seo, …, Y. H. Lee. 2003. Tip-functionalized carbon nanotubes under electric fields. *Phys. Rev. B.* 68:115403.
38. Brooks, B. R., R. E. Bruccoleri, …, M. Karplus. 1983. CHARMM: a program for macromolecular energy, minimization, and dynamics calculations. *J. Comput. Chem.* 4:187–217.
39. von Rague Schleyer, P., P. R. Schreiner, …, H. F. Schaefer III, editors. 1998., The Encyclopedia of Computational Chemistry, Vol. 1. John Wiley & Sons, Chichester, UK.
40. Allen, T. W., T. Baştuğ, …, S. H. Chung. 2003. Gramicidin A channel as a test ground for molecular dynamics force fields. *Biophys. J.* 84:2159–2168.
41. Hou, S., Z. Shen, …, Z. Xue. 2003. Quantum chemistry study on the open end of single-walled carbon nanotubes. *Chem. Phys. Lett.* 373:308–313.
42. Hilder, T. A., R. Yang, …, S. H. Chung. 2010. On validity of current force fields for simulations on boron nitride nanotubes. *Micro. Nano Lett.* 5:150–156.
43. Farhat, S., M. L. de La Chapelle, …, P. Bernier. 2001. Diameter control of single-walled carbon nanotubes using argon-helium mixture gases. *J. Chem. Phys.* 115:6752–6758.
44. Nikolaev, P., M. J. Bronikowski, …, R. E. Smalley. 1999. Gas-phase catalytic growth of single-walled carbon nanotubes from carbon monoxide. *Chem. Phys. Lett.* 313:91–97.
45. Li, Z. M., J. P. Zhai, …, Z. K. Tang. 2004. Synthesis of 4 Å single-walled carbon nanotubes in catalytic Si-substituted $AlPO_4$-5 molecular sieves. *Appl. Phys. Lett.* 85:1253–1255.
46. Humphrey, W., A. Dalke, and K. Schulten. 1996. VMD: visual molecular dynamics. *J. Mol. Graph.* 14:33–38.
47. Nielsen, S. O., B. Ensing, …, M. L. Klein. 2005. Lipid bilayer perturbations around a transmembrane nanotube: a coarse grain molecular dynamics study. *Biophys. J.* 88:3822–3828.
48. Kastenholz, M. A., and P. H. Hünenberger. 2004. Influence of artificial periodicity and ionic strength in molecular dynamics simulations of charged biomolecules employing lattice-sum methods. *J. Phys. Chem. B.* 108:774–788.
49. Kumar, S., J. M. Rosenberg, …, P. A. Kollman. 1995. Multidimensional free-energy calculations using the weighted histogram analysis method. *J. Comput. Chem.* 16:1339–1350.
50. Grossfield, A. An implementation of WHAM: the weighted histogram analysis method. http://membrane.urmc.rochester.edu/Software/WHAM/WHAM.html. Accessed 20 August 2008.
51. Jarzynski, C. 1997. Nonequilibrium equality for free energy differences. *Phys. Rev. Lett.* 78:2690–2693.
52. Kuyucak, S., O. S. Andersen, and S. H. Chung. 2001. Models of permeation in ion channels. *Rep. Prog. Phys.* 64:1427–1472.
53. Hoyles, M., S. Kuyucak, and S. H. Chung. 1998. Computer simulation of ion conductance in membrane channels. *Phys. Rev. E.* 58:3654–3661.
54. Shi, X., Y. Kong, and H. Gao. 2008. Coarse-grained molecular dynamics and theoretical studies of carbon nanotubes entering cell membrane. *Acta Mech. Sin.* 24:161–169.
55. Lopez, C. F., S. O. Nielsen, …, M. L. Klein. 2005. Structure and dynamics of model pore insertion into a membrane. *Biophys. J.* 88:3083–3094.
56. Chung, S. H., T. W. Allen, and S. Kuyucak. 2002. Conducting-state properties of the KcsA potassium channel from molecular and Brownian dynamics simulations. *Biophys. J.* 82:628–645.
57. Ng, J. A., T. Vora, …, S. H. Chung. 2008. Estimating the dielectric constant of the channel protein and pore. *Eur. Biophys. J.* 37:213–222.
58. Andersen, O. S., R. E. Koeppe, 2nd, and B. Roux. 2005. Gramicidin channels. *IEEE Trans. Nanobiosci.* 4:10–20.